

Stability Analysis of Parallel DC-DC Converters

SUDIP K. MAZUMDER, Senior Member, IEEE
University of Illinois at Chicago

We develop analytic methodologies for stability analyses (using nonlinear and linear methodologies) of parallel dc-dc converters (under unsaturated and saturated operating conditions) using their switching model, discrete model (based on nonlinear map), and averaged model. We describe the approach for investigating the behavior of the stable and unstable equilibrium solutions of a parallel dc-dc converter under parametric variations and illustrate the methodology using a load-sharing dc-dc buck converter. For unsaturated operating condition, using bifurcation analysis and Floquet theory, we predict the stability boundary of the nominal solution, determine its postinstability dynamics, and investigate the dependence of the converter dynamics on its initial conditions. Subsequently, we demonstrate the differences in the predictions of the instabilities and instability boundaries using (conventional) linearized averaged (small-signal) and discrete and switching models.

Manuscript received September 27, 2003; revised May 31 and September 3, 2005; released for publication September 3, 2005.

IEEE Log No. T-AES/42/1/870591.

Refereeing of this contribution was handled by W. M. Polivka.

This work was supported in part by the National Science Foundation CAREER Award received by Professor Mazumder in 2003 under Award 0239131.

Author's address: Dept. of Electrical and Computer Engineering, MC 154, 1020 Science and Engineering Offices, University of Illinois at Chicago, 851 S. Morgan St., Chicago, IL 60607-7053, E-mail: (mazumder@ece.uic.edu).

0018-9251/06/\$17.00 © 2006 IEEE

I. INTRODUCTION

Parallel dc-dc converters are widely used in telecommunication power supplies [32]. They operate under closed-loop feedback control to regulate the output voltage and enable load sharing. These closed-loop converters are inherently nonlinear systems. The major sources of nonlinearities are the switching nonlinearity and converter interaction. So far, however, analyses in this area of power electronics are based primarily on linearized (small-signal) averaged models. When a nonlinear converter has solutions other than the nominal one, small-signal analyses cannot predict the basin of attraction of the nominal solution and the dynamics of the system after the nominal solution loses stability. The dependence of the converter dynamics on the initial conditions is also ignored in small-signal analyses. In addition, averaged models cannot predict the dynamics of a switching converter in a saturated region.

To analyze the stability of these switching systems, one has to deal first with their discontinuity [24, 31]. The concept of stability of the equilibrium solutions of a continuous, smooth system is well defined [1, 2]. However, for discontinuous systems, the definition of solution is itself not straightforward [3–5]. To analyze the stability of an n -dimensional discontinuous system with m switching planes, one has to first define a region of operation, which in general lies at the intersection of these m hyperplanes. The global stability of this region is defined as follows [4]. One has to show first that all of the trajectories approach this region (reaching condition) and that, once on this hypersurface, they cannot leave it (existence condition). If these two conditions are satisfied, then the discontinuous system has a solution surface or a sliding mode. The dynamics of the system on this hypersurface is described by a set of equations, which are smooth and continuous. Finally, one has to show that all of the solutions on this surface tend to a single equilibrium point as time $t \rightarrow \infty$.

Analysis of a variable-structure system using an averaged model assumes two things. First, a solution surface exists. In other words, the reaching and existence conditions are satisfied. Second, the control has no delay or the switching frequency is infinite. In reality, the switching frequency is finite and for many converters global existence of a solution surface for any controller is not possible.

If the frequency is finite, then we do not have a solution surface but a boundary layer around it [5]. Thus stability in the sense of Filippov [4] can be applied only if the width of the boundary layer is zero. Under this condition, the dynamics of the system on the solution surface are described accurately by the averaged model. However, when the width of the boundary layer is not zero, we convert the periodic system to a map. Thus, within the boundary layer, we

redefine the stability problem from one of analyzing the stability of a periodic orbit to that of analyzing the stability of a fixed point.

We use these basic concepts to investigate the local and global stabilities of nonlinear, nonautonomous parallel dc-dc converters in the unsaturated and saturated regions.¹ Unlike [32] and [33], the analyses presented here are generalized and the concept feasibility is illustrated for a simple two-converter problem using commonly-used averaged-current sharing control instead of master-slave control in [33]. The present paper also outlines stability approaches using switching, discrete, and averaged model for parallel dc-dc converters. Further, unlike [32] and [33], the analyses have been presented here for unsaturated as well saturated regions. Within the unsaturated region, we develop techniques to predict the fast-scale and slow-scale stability boundaries and to determine the type of instability of the nominal orbit. Using these ideas, instabilities of two closed-loop buck converters operating in phase and with interleaving are investigated, which is also a key difference of the present work compared with [33]. For these two cases, we compare the results obtained using a nonlinear map with those obtained using the averaged model and demonstrate the shortcomings of the latter. Unlike [33], we also demonstrate the impact of parametric variations of the parallel converter on its fast-scale and slow-scale instabilities. Finally, we investigate the impact of a strong feedforward disturbance on the stability of the two buck converters when they have the same parameters and when they have parametric variation. Using concepts developed in this paper, we predict the dynamics of the converter in the saturated and unsaturated regions under steady-state and transient conditions. The presented stability problem is a real phenomenon, which could occur in any practical multi-module converter system and the results presented can be used to predict and prevent such a problem.

II. MODELING

A. Power Stage

We assume that the nonlinearities due to the power devices and parasitics are negligible and that the converter, operating in continuous conduction mode (CCM),² is clocked at a rate equal to the

¹A comprehensive stability analysis using nonlinear map for a single dc-dc converter (i.e., $N = 1$ in Section II) is provided in [9].

²If the parallel dc-dc operates in discontinuous conduction mode (DCM), the map-based analysis approach described here remains exactly the same; only the map and the auxiliary switching conditions change. Likewise, the switching and the averaged models of the parallel dc-dc converters will change, but the basic stability analysis approach remains unchanged.

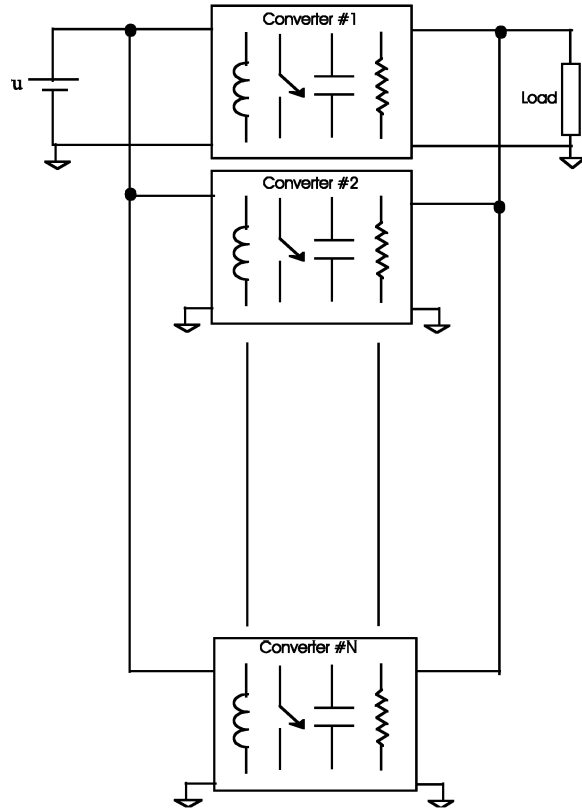


Fig. 1. Generic configuration of N parallel dc-dc converters operating with single voltage source and load.

switching frequency. Moreover, the controller is designed in such a way that, once a change of state is latched, it can be reset only by the next clock. This effectively eliminates the possibility of multiple pulses within a switching cycle. In Fig. 1 we show a schematic of a generic basic parallel dc-dc converter with one switch per converter. The total number of converters connected in parallel is N . Each individual module within these multi-topological systems is in the on-state when the switch is closed and in the off-state when it is open. We represent these switching functions by a switching vector $S(t)$. We assume that the phase shift between the carrier waveforms of two successive converters is equal to $\delta = T/N$, which is constant (where T is the switching cycle time). We note that, when $\delta = 0$, the converters are switching in phase. If we represent the states of the open-loop converter (i.e., the inductor currents $i_{L_i}(t)$ and the capacitor voltages $v_{C_i}(t)$ by the vector $X^o(t)$, then the equations governing a parallel-boost or a parallel-buck converter can be expressed as

$$\begin{aligned} \dot{X}^o(t) &= F_1^o(X^o(t), u(t), S(t)) \\ v_{dc}(t) &= F_2^o(X^o(t), u(t), S(t)) \end{aligned} \quad (1)$$

where $u(t)$ is the forcing input. Equation (1) represents a discontinuous and nonautonomous system. The

discontinuity is due to the switching vector $S(t)$. For convenience, we drop the notation of time from now on and rewrite (1) as

$$\begin{aligned}\dot{X}^o &= F^o(X^o, u) + G^o(X^o, u)S + W_1^o(X^o, S) \\ v_{dc} &= H^o(X^o) + W_2^o(X^o, S)\end{aligned}\quad (2)$$

where F^o , G^o , and H^o are continuous functions. For some systems (e.g., the parallel-buck converter), W_1^o and W_2^o are continuous because terms containing the equivalent series resistance (ESR) are not coupled with the switching function. Hence, W_1^o and W_2^o can be lumped with the other terms in (2). However, for other systems like the parallel-boost converter, they are discontinuous. If we neglect the ESR, then (2) simplifies to the following form:

$$\begin{aligned}\dot{X}^o &= F^o(X^o, u) + G^o(X^o, u)S \\ v_{dc} &= H^o(X^o).\end{aligned}\quad (3)$$

Equations (2) and (3) represent generic switching models of parallel-buck and parallel-boost converters when the effect of the ESR is incorporated and when it is not.

An alternate way to model the variable-structure system represented by (2) is to use a map [6–9]. Because there are N converters (as illustrated in Fig. 2 for $N = 2$), which are operating in parallel with a phase shift of δ , there are N switchings that occur in each switching cycle (of duration T) of the nominal steady-state system. The state-space equations for the i th subswitching cycle of duration t_i are written as

$$\begin{aligned}\dot{X}^o &= A_i^o X^o + B_i^o u \\ v_{dc} &= C_i^o X^o\end{aligned}\quad (4)$$

where

$$\sum_{i=1}^N t_i = T \quad (5)$$

and A_i^o , B_i^o , and C_i^o are matrices that describe the open-loop system in the time interval t_i [9]. In each switching subcycle, these matrices can be obtained from (2) by substituting an appropriate vector consisting of binary numbers for the switching vector S .

Next, we derive an exact solution of the open-loop system by stacking the consecutive solutions of (4) over a switching period. The resulting discrete-time equation can be written in state-space form as

$$\begin{aligned}X_{k+1}^o &= f_1^o(X_k^o, t_1, t_2, \dots, t_{2N}, u_k) \\ &= \Phi^o(t_1, t_2, \dots, t_{2N})X_k^o + \Gamma^o(t_1, t_2, \dots, t_{2N})u_k \\ v_{dc_{k+1}} &= f_2^o(X_k^o, t_1, t_2, \dots, t_{2N}, u_k) = C_{2N}^o X_{k+1}^o\end{aligned}\quad (6)$$

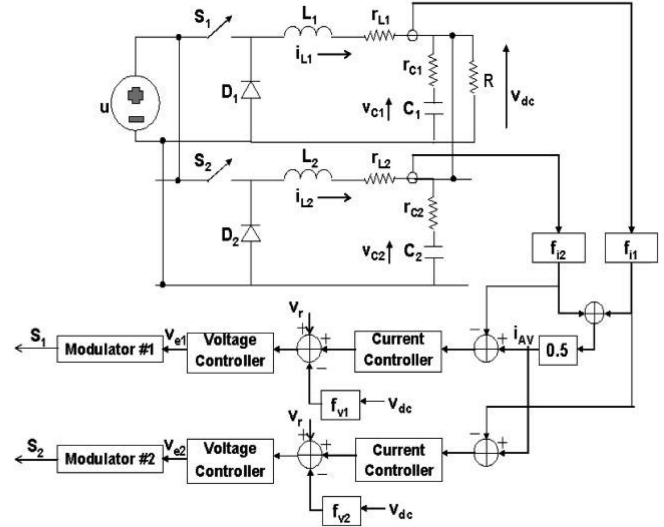


Fig. 2. Two parallel buck converters operating with (averaged) ACS control. If controllers for the two converters use only inductor current and capacitor voltages for feedback, then they are described as static-feedback controllers. If however, controllers use additional states, then they are described as dynamic-feedback controllers. We analyzed the stability and dynamics of the parallel buck converter under unsaturated mode of operation using a (conventionally used) dynamic feedback controller [9]. For saturated mode of operation, we used a simple static-feedback controller to illustrate the dynamics and instabilities in simple terms.

where

$$\begin{aligned}\Phi^o(t_1, t_2, \dots, t_{2N}) \\ = \prod_{i=1}^{2N} \Phi_{2N-i+1}^o(t_i) \quad \text{and} \quad \Phi_{2N-i+1}^o(\tau) = e^{A_{2N-i+1}^o \tau}\end{aligned}\quad (7a)$$

$$\begin{aligned}\Gamma^o(t_1, t_2, \dots, t_{2N}) \\ = \left(\prod_{i \neq 1}^{2N} \Phi_{2N-i+1}^o \right) \int_0^{t_1} \Phi_1^o(\tau) B_1^o d\tau \\ + \left(\prod_{i \neq 1,2}^{2N} \Phi_{2N-i+1}^o \right) \int_0^{t_2} \Phi_2^o(\tau) B_2^o d\tau + \dots \\ + \int_0^{t_{2N}} \Phi_{2N}^o(\tau) B_{2N}^o d\tau\end{aligned}\quad (7b)$$

$$t_j = \delta - t_{j-1} \quad \forall \quad j = 2, 4, \dots, 2N \quad \text{and} \quad \sum_{i=1}^N t_i = T. \quad (7c)$$

Using

$$\int_0^t e^{A_i^o \tau} B_i^o d\tau = (e^{A_i^o t} - I)(A_i^o)^{-1} B_i^o \quad (8)$$

and (7), we simplify the expression for X_{k+1}^o in (6) to

$$\begin{aligned}
X_{k+1}^o &= f_1^o(X_k^o, t_1, t_2, \dots, t_{2N}, u_k) \\
&= \prod_{i=1}^{2N} e^{A_i^o t_{N-i+1}} X_k^o \\
&\quad + \left(\begin{aligned} &\left(\prod_{i \neq 1}^{2N} e^{A_i^o t_i} \right) (e^{A_1^o t_1} - I)(A_1^o)^{-1} B_1^o \\ &+ \left(\prod_{i \neq 1,2}^{2N} e^{A_i^o t_i} \right) (e^{A_2^o t_2} - I)(A_2^o)^{-1} B_2^o \\ &+ \dots + (e^{A_{2N}^o t_{2N}} - I)(A_{2N}^o)^{-1} B_{2N}^o \end{aligned} \right) u_k.
\end{aligned} \tag{9}$$

Equations (6) and (9) describing $v_{dc_{k+1}}$ and X_{k+1}^o represent a map for dc-dc parallel-buck and parallel-boost converter. If we compare the map with the switching model described in (2), we see that the map does not have the discontinuities due to the switching vector S . This helps in studying the dynamics because the concept of solution for smooth systems is well defined. Besides, simulations based on this map are much faster since they correlate the states in one switching cycle (of duration T) with those in the next switching cycle. Because the map is not dependent on time any more, it describes a reduced-order system. Hence, it cannot predict the dynamics of a parallel converter beyond half the switching frequency. However, it can predict the subharmonics accurately.

Another approach to modeling parallel converters is based on state-space averaging [10, 11]. In this case, we convert the discontinuous-differential system of equations described by (2) to a continuous system by replacing the vector representing the switching functions with a smooth and continuous duty-ratio vector. In Appendix A, we illustrate the derivation of an averaged model with two examples based on a parallel-buck converter operating with two different switching schemes. The general expression for the averaged model is

$$\begin{aligned}
\dot{\bar{X}}^o &= F^o(\bar{X}^o, \bar{u}) + G^o(\bar{X}^o, \bar{u}) + W_{1av}^o(\bar{X}^o, D) \\
\bar{v}_{dc} &= H^o(\bar{X}^o) + W_{2av}^o(\bar{X}^o, D)
\end{aligned} \tag{10}$$

where W_{1av}^o and W_{2av}^o are continuous functions and \bar{X}^o represents the averaged value of the open-loop states. The symbol D is a vector, which denotes the duty ratios of a parallel converter. For some converters (e.g., parallel buck), W_{1av}^o and W_{2av}^o are independent of D . Hence, they can be lumped with F^o and H^o . However, for others, like parallel boost converters, they depend on D . Equation (10), describes a system of ordinary differential equations, which can be used for investigating only slow-scale dynamics.

B. Controller

There are more than one scheme for paralleling dc-dc converters [27–30], including the master-slave method [12] and the active-current sharing method [13, 14]. The objectives of all of these schemes, in general, are to regulate the output voltage and share the load power equally among the converters. The stability techniques we develop here are generic. However, due to lack of space, we present simulation results for the performance of parallel converters operating with an active-current sharing (ACS) scheme.

In Fig. 2, we show a schematic for an ACS control. The symbol i_{av} represents the average of all load currents. To share the load equally among the converters, the error between i_{av} and the load current supplied by each converter is added to the reference voltage v_r . The updated voltage reference is then compared with the output voltage for each converter. The output of the voltage loop is compared with the inductor current, which is the controller error signal. The controller can be simplified on the need and application. If we consider a static-feedback controller, then the expression of the error signal for each converter can be expressed as

$$v_{e_i} = P_i^s X^o + v_r \tag{11}$$

where P_i^s is a matrix corresponding to the static-feedback controller. If, however, we consider a dynamic-feedback controller, then we obtain

$$v_{e_i} = P_i^d X^c. \tag{12}$$

In (12), X^c represents the additional states of the dynamics-feedback controller and is given by

$$\dot{X}^c = A^c X^{aug} + B^c u + B^{rc} v_r \tag{13}$$

where $X^{aug} = (X^o \ X^c)^T$, A^c is a matrix, and B^c and B^{rc} are column vectors. Equations (11)–(13) give the expressions for a multiloop static/dynamic feedback controller. If the multiloop system does not use an inner inductor-current loop then the matrices in (11)–(13) have to be modified.

III. CLOSED-LOOP PARALLEL DC-DC CONVERTER

For a static-feedback controller, the order of the closed-loop and open-loop systems remains the same. The closed-loop switching model for the parallel converter is given by

$$\begin{aligned}
\dot{X} &= F(X, u, v_r) + G(X, u)S + W_1(X, S) \\
v_{dc} &= H(X) + W_2(X, S)
\end{aligned} \tag{14}$$

where F , G , and H are continuous functions. The functions W_1 and W_2 are continuous for the

parallel-buck converter and discontinuous for the parallel-boost converter. For a static-feedback controller, $X = X^o$. But for a dynamic-feedback controller $X = X^{\text{aug}}$. The individual components of the switching vector S are given by

$$s_i = \Omega_i(v_{e_i} - v_{\text{ramp}_i}(t, \delta)) \quad (15)$$

where individual ramp signals are described as follows:

$$v_{\text{ramp}_i}(t, \delta) = v_{m_i} * \text{mod}(t + (i-1)\delta, T) * f \quad (16)$$

$$\forall i = 1, \dots, N \quad \text{and} \quad f = 1/T.$$

Equation (16) describes the equations for carrier waveforms with amplitudes v_{m_i} . Each of these ramp waveforms has a period of T . Between the two carrier waveforms, there is a phase shift δ . It follows from (15) that the s_i are functions of the states of the closed-loop converter. Hence, the closed-loop switching model in (14) represents a nonlinear nonautonomous discontinuous system.

Next, we derive a nonlinear map based on (14). The state-space equation for the i th subswitching cycle (of duration t_i) is written as

$$\dot{X} = A_i X + B_i u + B_i^r v_r \quad (17)$$

$$v_{\text{dc}} = C_i X$$

where

$$\sum_{i=1}^N t_i = T \quad (18)$$

and A_i , B_i , B_i^r , and C_i and are matrices that describe the closed-loop system in each subcycle. In each switching subcycle, these matrices can be obtained from (14) by substituting an appropriate vector consisting of binary numbers for the switching vector S . Next, we derive an exact solution of the closed-loop system by stacking the consecutive solutions of (17) over a switching period. The resulting discrete-time difference equation can be written in state-space form as

$$X_{k+1} = f_1(X_k, t_1, t_2, \dots, t_{2N}, u_k)$$

$$= \prod_{i=1}^{2N} e^{A_i t_i} X_k + \left(\begin{array}{l} \left(\prod_{i \neq 1}^{2N} e^{A_i t_i} \right) (e^{A_1 t_1} - I)(A_1)^{-1} B_1 \\ + \left(\prod_{i \neq 1, 2}^{2N} e^{A_i t_i} \right) (e^{A_2 t_2} - I)(A_2)^{-1} B_2 \\ + \dots + (e^{A_{2N} t_{2N}} - I)(A_{2N})^{-1} B_{2N} \end{array} \right) u_k$$

$$+ \left(\begin{array}{l} \left(\prod_{i \neq 1}^{2N} e^{A_i t_i} \right) (e^{A_1 t_1} - I)(A_1)^{-1} B_1^r \\ + \left(\prod_{i \neq 1, 2}^{2N} e^{A_i t_i} \right) (e^{A_2 t_2} - I)(A_2)^{-1} B_2^r \\ + \dots + (e^{A_{2N} t_{2N}} - I)(A_{2N})^{-1} B_{2N}^r \end{array} \right) v_r \quad (19a)$$

$$v_{\text{dc}_{k+1}} = f_2(X_k, t_1, t_2, \dots, t_{2N}, u_k, v_r) = C_{2N} X_{k+1} \quad (19b)$$

$$\sigma(X_k, t_1, t_2, \dots, t_{2N}, u_k, v_r) = 0 \quad (19c)$$

and

$$t_j = \delta - t_{j-1} \quad \forall j = 2, 4, \dots, 2N. \quad (19d)$$

In (19c), σ is a vector of dimension $N \times 1$ and represents the auxiliary switching conditions for all of the converters. For instance, the switching condition for the converter that switches first is given by

$$\sigma(X_k, t_1, u_k, v_r) = \varphi - (e^{A_1 t_1} \Psi_k + (e^{A_1 t_1} - I)A_1^{-1}(B_1 u_k + B_1^r v_r)) - v_{\text{ramp}_1} t_1 = 0 \quad (20)$$

where the vector φ represents the controller. Using (19d), we reduce the dimension of σ to N .

Finally, we obtain an averaged model for the closed-loop system. Using the same methodology, which was used to develop the averaged model for the open-loop converter, we show that the closed-loop averaged model for the parallel converter is given by the following expressions:

$$\dot{\bar{X}} = F(\bar{X}, \bar{u}, v_r) + G(\bar{X}, \bar{u})D + W_{1_{\text{av}}}(\bar{X}, D)$$

$$\bar{v}_{\text{dc}} = H(\bar{X}) + W_{2_{\text{av}}}(\bar{X}, D) \quad (21)$$

$$d_i = \frac{1}{v_{\text{ramp}_i}} \bar{v}_{e_i} = P_i \bar{X}$$

where $W_{1_{\text{av}}}$ and $W_{2_{\text{av}}}$ are continuous functions, P_i represents a matrix, and D is a vector representing the duty ratios of the converters operating in parallel. The individual components of this vector D are given by d_i in (21). Equation (21) represents a nonlinear averaged model. It can be used for studying the slow-scale instability. If the ESRs of the output capacitors are neglected, the averaged model cannot distinguish between the dynamics of interleaved and synchronized converters. Moreover, the averaged model cannot be used to study the impact of saturation.

IV. ANALYSIS

In this section, we show how to analyze the local and global stability of the dynamics of a parallel dc-dc converter operating in the unsaturated and saturated regions. The parallel converters, shown in Fig. 1, operate with a finite switching frequency.

The dynamics of these discontinuous nonlinear nonautonomous systems evolve on fast and slow scales. The stability analysis of these discontinuous systems is difficult because the definition of a solution is not clearly defined.

Filippov [4] and Aubin and Cellina [3] proposed differential inclusion to find solutions of such discontinuous systems with a multivalued right-hand side. The resulting solution of this set-valued map describes a solution of the slow dynamics [3]. The averaged model in (21) approximately describes the slow dynamics for two reasons. First, the switching frequencies of the systems are finite. Hence, they do not have a discontinuous surface but a boundary layer around the discontinuity. The averaged model in (21) is based on the assumption of an infinite frequency and hence the width of the boundary layer is zero. Second, because switching of the converters in Figs. 1 and 2 is based on a comparison of an error signal with a ramp rather than a hysteresis, the equivalent control approach proposed by Filippov (which forms the basis for (21)) is not always directly applicable [5]. However, an analysis using an averaged model is straightforward because it is continuous and smooth. We deal with the stability based on an averaged model later in this section.

An alternate way to analyze the stability of these variable-structure systems is to use the nonlinear map in (19). We describe the evolution of the discontinuous system as a sequence. Besides, we eliminate the discontinuity due to switching by predicting the states at the beginning of the next switching cycle based on the information available at the end of the current switching cycle. Using these maps, we convert the problem of finding the stability of a nominal orbit (period-one orbit) to that of finding the stability of a fixed point.

Another way to investigate the stability of the nominal solution of (14) is numerical computation. We transform (14) to the following form:

$$X_{k+1} = M_1(X_k, t'_k, t'_{k+1}, u_k, v_r). \quad (22)$$

By choosing a relatively small time step $t'_{k+1} - t'_k$, one can obtain a fairly accurate solution. In (22), the scalar t' represents the actual time and not the instant of switching. How small the time step has to be depends on how fast the open-loop and closed-loop states evolve. The degree of accuracy depends not only on the time step but also on the type of numerical algorithm [15]. It was found that the use of a combination of implicit and explicit numerical techniques gives the best results. The rationale behind obtaining the solution of a discontinuous system using numerical integration is provided by the Lebesgue measure theory [16]. There are two primary reasons why it is applicable here. First, the total number of switchings in one switching cycle is finite because multiple pulsing cannot occur. Second, at each of

these switching instants, the right- and left-hand limits of each of the states of the converters are equal. This is because we are considering hard-switched converters. Thus, at the points of discontinuity, we do not have any jump in the states. Based on these two pieces of information and on whether the sampling time for numerical integration is much smaller than the dynamics of the system, the Lebesgue theory tells us that we can consider the points of discontinuities (due to switchings) to have zero measure [4, 16]. In other words, though the system is undefined at the points of switching, we can carry out the integration and the resulting solution is valid almost everywhere.

A. Stability Analysis using the Switching Model

We use a combination of a shooting technique and Newton-Raphson procedure to calculate the periodic orbits and determine their stability. To accomplish this, we convert the initial-value problem in (14) to a two-point boundary-value problem. Let the dimension of X be $n \times 1$. We seek an initial condition $\gamma = X(0)$ such that the minimal solution $X(t, \gamma)$ of (14) satisfies the condition

$$X(T, \gamma) = \gamma = X(0). \quad (23)$$

In other words, the trajectory that runs from $\gamma = X(0)$ to the same location over a time period of T represents the desired periodic solution.

We start with a guess γ_0 and seek a $\delta\gamma$ such that

$$X(T, \gamma_0 + \delta\gamma) - (\gamma_0 + \delta\gamma) \approx 0. \quad (24)$$

Expanding (24) in a Taylor series and keeping only the linear terms in $\delta\gamma$, we obtain

$$(\partial X_\gamma(T, \gamma_0) - I)\delta\gamma = \gamma_0 - X(T, \gamma_0). \quad (25)$$

In (25), $\partial X_\gamma(T, \gamma_0)$ represents the derivatives of X with respect to γ evaluated at (T, γ_0) . The dimension of the matrix $\partial X_\gamma(T, \gamma_0)$ is $n \times n$. The individual components of this matrix are given by

$$\partial X_{\gamma_i}(T, \gamma_0) = \lim_{h \rightarrow 0} \frac{X^i(T, \gamma_0 + h\gamma_{0i}) - X(T, \gamma_0)}{h}. \quad (26)$$

Once $\partial X_\gamma(T, \gamma_0)$ is known, we solve the system of n linear algebraic (25) for $\delta\gamma$. Then, we use $\delta\gamma$ to update the initial guess γ_0 and repeat the process until $\delta\gamma$ is within a tolerance level. Finally, the stability of the calculated periodic solution is ascertained from the eigenvalues of the monodromy matrix ∂X_γ evaluated at (T, γ_0) . For the periodic solution to be asymptotically stable, every eigenvalue but one must be inside the unit circle in the complex plane.

B. Stability Analysis using the Discrete Model

Let us assume that the closed-loop system described by (19) is operating in steady state. The

fixed points of X_k in (19a) correspond to period-one orbits of the closed-loop converter. They are obtained using the constraint $X_{k+1} = X_k = X_s$. Letting $u_s = u_k$, $t_1 = t_{1s}$, $t_2 = t_{2s}, \dots, t_{2N} = t_{2Ns}$ we find that the fixed points of (19a) are given by

$$X_s = \left(I - \prod_{i=1}^{2N} e^{A_{2N-i+1} t_{i_s}} \right)^{-1} \times \left(\begin{array}{l} \left(\prod_{i \neq 1}^{2N} e^{A_{2N-i+1} t_{i_s}} \right) (e^{A_1 t_{1s}} - I)(A_1)^{-1} B_1 \\ + \left(\prod_{i \neq 1,2}^{2N} e^{A_{2N-i+1} t_{i_s}} \right) (e^{A_2 t_{2s}} - I)(A_2)^{-1} B_2 \\ + \dots + (e^{A_{2N} t_{2Ns}} - I)(A_{2N})^{-1} B_{2N} \end{array} \right) u_s + \left(I - \prod_{i=1}^{2N} e^{A_{2N-i+1} t_{i_s}} \right)^{-1} \times \left(\begin{array}{l} \left(\prod_{i \neq 1}^{2N} e^{A_{2N-i+1} t_{i_s}} \right) (e^{A_1 t_{1s}} - I)(A_1)^{-1} B_1^r \\ + \left(\prod_{i \neq 1,2}^{2N} e^{A_{2N-i+1} t_{i_s}} \right) (e^{A_2 t_{2s}} - I)(A_2)^{-1} B_2^r \\ + \dots + (e^{A_{2N} t_{2Ns}} - I)(A_{2N})^{-1} B_{2N}^r \end{array} \right) v_r. \quad (27)$$

Substituting (27) into (19c), we obtain

$$\sigma(X_s, t_{1s}, t_{2s}, \dots, t_{2Ns}, u_s, v_r) = 0. \quad (28)$$

We solve (27) and (28) for the N unknowns X and the t_{i_s} . One way to solve for the unknowns is to substitute for X_s from (27) into (28) and solve for the t_{i_s} . Once the t_{i_s} are calculated, we solve for X_s . This is difficult for higher order systems because most of the mathematical packages, like Matlab or Mathematica, cannot symbolically compute exponents of very large matrices. Besides, the computation of $(I - \prod_{i=1}^{2N} e^{A_{2N-i+1} t_{i_s}})$ in (27) using these packages is inaccurate. Alternately, we use a Newton-Raphson method. We start with an initial guess X_g and t_{i_g} for the steady-state values of X_s and t_{i_s} . This guess is obtained using either simulation or the method of steepest decent [17]. Keeping the u_k constant, we rewrite (19a) and (19c) as

$$X_g + \delta X_g = f_1(X_g + \delta X_g, t_{1g} + \delta t_{1g}, t_{2g} + \delta t_{2g}, \dots, t_{2Ng} + \delta t_{2Ng}) \quad (29)$$

$$\sigma(X_g + \delta X_g, t_{1g} + \delta t_{1g}, t_{2g} + \delta t_{2g}, \dots, t_{2Ng} + \delta t_{2Ng}) = 0. \quad (30)$$

Expanding (29) and (30) in Taylor series, we obtain

$$X_g + \delta X_g = f_1(X_g + \delta X_g) + \frac{\partial f_1}{\partial X_g} \delta X_g + \frac{\partial f_1}{\partial t_g} \delta t_g \quad (31)$$

$$\sigma(X_g + \delta X_g) + \frac{\partial \sigma}{\partial X_g} \delta X_g + \frac{\partial \sigma}{\partial t_g} \delta t_g = 0 \quad (32)$$

where t_g is a vector representing $t_{1g}, t_{2g}, \dots, t_{2Ng}$. We rewrite (31) and (32) as

$$\begin{pmatrix} \frac{\partial f_1}{\partial X_g} & \frac{\partial f_1}{\partial t_g} \\ \frac{\partial \sigma}{\partial X_g} & \frac{\partial \sigma}{\partial t_g} \end{pmatrix} \begin{pmatrix} \delta X_g \\ \delta t_g \end{pmatrix} = J \begin{pmatrix} \delta X_g \\ \delta t_g \end{pmatrix} = \begin{pmatrix} X_g - f_1 \\ -\sigma \end{pmatrix}. \quad (33)$$

Equation (33) represents a set of linear algebraic equations, which are solved for δX_g and δt_g by using the LU decomposition method [18]. To this end, we express J as LU , where the matrices L and U represent the lower and upper triangular matrices of J . Then, we rewrite (33) as

$$J \begin{pmatrix} \delta X_g \\ \delta t_g \end{pmatrix} = LU \begin{pmatrix} \delta X_g \\ \delta t_g \end{pmatrix} = \begin{pmatrix} X_g - f_1 \\ -\sigma \end{pmatrix}. \quad (34)$$

Multiplying (34) from the left with L^{-1} , we have

$$U \begin{pmatrix} \delta X_g \\ \delta t_g \end{pmatrix} = Z = L^{-1} \begin{pmatrix} X_g - f_1 \\ -\sigma \end{pmatrix} \quad (35)$$

which can be solved for the new set of variables Z . Then the $(\delta X_g \ \delta t_g)$ are calculated without inverting the matrix U .

We found that, unlike the matrix J^{-1} , the matrix L^{-1} can always be computed correctly by either Matlab or Mathematica. If, however, this is not the case, then one can use more advanced algorithms, such as the conjugate gradient method [18] and globally convergent homotopy algorithms [19]. However, homotopy algorithms have the disadvantage of giving both the real-valued as well as the complex-valued solutions.

To ascertain the stability of a given fixed point, we perturb the nominal values as

$$X = X_s + \delta X, \quad t = t_s + \delta t \quad (36)$$

$$u = u_s + \delta u, \quad v_{dc} = v_{dc_s} + \delta v_{dc}.$$

Substituting (36) into (19a) and (19c), expanding the results in Taylor series, and keeping first-order terms, we obtain

$$\delta X_{k+1} = \frac{\partial f_1}{\partial X} \delta X + \frac{\partial f_1}{\partial u} \delta u \quad (37)$$

$$\frac{\partial \sigma}{\partial X} \delta X + \frac{\partial \sigma}{\partial t} \delta t + \frac{\partial \sigma}{\partial u} \delta u = 0.$$

It follows from the second equation of (37) that

$$\delta t = - \left(\frac{\partial \sigma}{\partial t} \right)^{-1} \left(\frac{\partial \sigma}{\partial X} \delta X + \frac{\partial \sigma}{\partial u} \delta u \right). \quad (38)$$

Substituting (38) into the first equation of (37), yields

$$\delta X_{k+1} = H_1 \delta X + H_2 \delta u \quad (39)$$

where

$$H_1 = \frac{\partial f_1}{\partial X} - \left(\frac{\partial \sigma}{\partial t} \right)^{-1} \frac{\partial \sigma}{\partial X} \quad (40)$$

$$H_2 = \frac{\partial f_1}{\partial u} - \left(\frac{\partial \sigma}{\partial t} \right)^{-1} \frac{\partial \sigma}{\partial u}.$$

The stability of a given fixed point can be ascertained by the eigenvalues (Floquet multipliers) of H_1 [1]. For asymptotic stability, all of the Floquet multipliers must be within the unit circle.

To determine the region of attraction of the nominal solution, we need to select a Lyapunov function $V(\cdot)$ for the nonlinear system in (19a) and a class K function α . If there is a ball $B(\tilde{X}^*)$ with radius r centered at \tilde{X}^* such that for all $\tilde{X}_k \in B(\tilde{X}^*)$, then the stability of the nominal solution of (19a) is guaranteed if [20]

$$V(\tilde{X}_k) \geq \alpha(\|\tilde{X}_k - \tilde{X}^*\|)$$

$$V(\tilde{X}_{k+1}) - V(\tilde{X}_k) < 0 \quad (41)$$

$$V(\tilde{X}^*) = 0$$

where $\tilde{X}_k = X_k - X_s$.

If one of the Floquet multipliers exits the unit circle through $+1$, then either a cyclic-fold, or a symmetry-breaking, or a transcritical bifurcation occurs. If a Floquet multiplier exits the unit circle through -1 , a period-doubling or flip bifurcation occurs. If, however, two of the Floquet multipliers exit the unit circle as complex conjugates, a secondary Hopf bifurcation occurs. To find out whether the bifurcation is subcritical or supercritical in nature, we calculate the normal form of the nonlinear system in the neighborhood of the bifurcation. Alternately, we can use numerical simulation.

Next, we describe briefly the procedure to determine the normal form of the map near the bifurcation. For a given bifurcation parameter (e.g., input voltage), let the nonlinear map describing the dynamics of the closed-loop converter be

$$X_{k+1} = f_1(X_k, t_k) = f_1(X_k, \Phi(X_k)) \quad (42)$$

$$\sigma(X_k, t_k) = \sigma(X_k, \Phi(X_k)) = 0 \quad (43)$$

where t_k is a vector representing $t_{1k}, t_{2k}, \dots, t_{2N_k}$. Expanding (42) about its nominal point using Taylor series and keeping terms up to third-order term, we

obtain

$$\hat{X}_{k+1} = \left(\frac{\partial f_1}{\partial X} + \frac{\partial f_1}{\partial \Phi} \frac{\partial \Phi}{\partial X} \right) \hat{X}_k$$

$$+ \frac{1}{2} \left(\frac{\partial^2 f_1}{\partial X^2} + \frac{\partial^2 f_1}{\partial \Phi \partial X} \frac{d\Phi}{dX} + \frac{\partial^2 f_1}{\partial X \partial \Phi} \frac{d\Phi}{dX} \right. \\ \left. + \frac{\partial^2 f_1}{\partial \Phi^2} \left(\frac{d\Phi}{dX} \right)^2 + \frac{\partial f_1}{\partial \Phi} \frac{d^2 \Phi}{dX^2} \right) \hat{X}_k^2$$

$$+ \frac{1}{6} \left(\frac{\partial^3 f_1}{\partial X^3} + \frac{\partial^3 f_1}{\partial \Phi \partial X^2} \frac{d\Phi}{dX} \right) \hat{X}_k^3$$

$$+ \frac{1}{6} \left(\frac{\partial^2 f_1}{\partial \Phi \partial X} + \frac{\partial^2 f_1}{\partial X \partial \Phi} \right) \left(\frac{d^2 \Phi}{dX^2} \right) \hat{X}_k^3$$

$$+ \frac{1}{6} \left(\frac{\partial^3 f_1}{\partial X \partial \Phi \partial X} + \frac{\partial^3 f_1}{\partial \Phi^2 \partial X} \frac{d\Phi}{dX} + \frac{\partial^3 f_1}{\partial X^2 \partial \Phi} \right. \\ \left. + \frac{\partial^3 f_1}{\partial \Phi \partial X \partial \Phi} \right) \left(\frac{d\Phi}{dX} \right) \hat{X}_k^3$$

$$+ \frac{1}{6} \left(\frac{\partial^3 f_1}{\partial X \partial \Phi^2} \left(\frac{d\Phi}{dX} \right)^2 + \frac{\partial^3 f_1}{\partial \Phi^3} \left(\frac{d\Phi}{dX} \right)^3 \right. \\ \left. + 2 \frac{\partial^2 f_1}{\partial \Phi^2} \left(\frac{d\Phi}{dX} \right) \left(\frac{d^2 \Phi}{dX^2} \right) \right) \hat{X}_k^3$$

$$+ \frac{1}{6} \left(\frac{\partial^2 f_1}{\partial X \partial \Phi} \frac{d^2 \Phi}{dX^2} + \frac{\partial^2 f_1}{\partial X^2} \frac{d\Phi}{dX} \frac{d^2 \Phi}{dX^2} + \frac{\partial f_1}{\partial \Phi} \frac{d^3 \Phi}{dX^3} \right) \hat{X}_k^3 \quad (44)$$

where Φ and its derivatives are calculated from (43).

Next, we let $X = W\xi$ (where W is a matrix whose column vectors are the eigenvectors of the linear term on the right-hand side of (44)) in (44) and obtain

$$\xi_{k+1} = J\xi_k + F_2(\xi_k) + F_3(\xi_k) + O(|\xi_k|^4) \quad (45)$$

where F_2 and F_3 represent the second-order and third-order nonlinear terms in ξ .

To determine the normal form of the map near a bifurcation resulting from a Floquet multiplier existing the unit circle either through $+1$ or -1 , we arrange the eigenvectors in W so that the eigenvector corresponding to this multiplier is the first. Hence, (45) can be rewritten as

$$\xi_{k+1}^1 = \alpha \xi_k^1 + F_2^1(\xi_k) + F_3^1(\xi_k) \quad (46)$$

$$\hat{\xi}_{k+1} = \alpha \hat{\xi}_k + \hat{F}_2(\xi_k) + \hat{F}_3(\xi_k) \quad (47)$$

where $\alpha = \pm 1$ and the vectors with the caret exclude the first elements. To calculate the center manifold, we let $\hat{\xi} = h(\xi^1)$, where h is a quadratic function vector of ξ_k^1 in (47) and obtain

$$h(\xi_{k+1}^1) = \hat{J}h(\xi_k^1) + \hat{F}_2(\xi_k^1, h(\xi_k^1)) + \hat{F}_3(\xi_k^1, h(\xi_k^1)). \quad (48)$$

Substituting (46) into (48) yields the functional

$$h(\alpha\xi_k^1) = \hat{J}h(\xi_k^1) + \hat{F}_2(\xi_k^2) + \dots \quad (49)$$

which can be solved for $h(\xi^1)$. Substituting for $h(\xi^1)$ in (46) yields the normal form

$$\hat{\xi}_{k+1}^1 = \alpha\hat{\xi}_k^1 + \hat{F}_2^1(\xi_k) + \hat{F}_3^1(\xi_k). \quad (50)$$

A similar procedure can be used to calculate the normal form in case two complex conjugate multipliers exist the unit circle.

C. Stability Analysis using the Averaged Model

The averaged model represents a continuous differential system, which is derived under the assumption of an infinite switching frequency. The closed-loop parallel converter described in the (21) may have more than one equilibrium solution. Therefore, in step one of our analysis, we determine the equilibrium solutions of equation of \dot{X} in (21) by setting $\dot{X} = 0$. The result is

$$\dot{X} = F(\bar{X}, \bar{u}, v_r) + G(\bar{X}, \bar{u})D + W_{1_{av}}(\bar{X}, D) = 0. \quad (51)$$

Substituting for the individual elements of D , i.e., d_i , from (21) into (51) yields a nonlinear system of algebraic equations for the \bar{X} . If there is only one equilibrium solution, which equals the nominal solution of the converter, then, based on the averaged model, we have a globally stable solution (in the unsaturated region). If there are more than one equilibrium solutions, then we need to determine the stability of the nominal solution. This is achieved by first linearizing the nonlinear system in the neighborhood of an equilibrium solution and then computing the eigenvalues of the Jacobian matrix. For stability, none of the eigenvalues of the Jacobian matrix should have a positive real part.

It follows from (11)–(13) that, if the feedback controller is static, the dimension of the closed-loop system, described by (21), is the same as the open-loop system, which is given by (10). However, in the case of a dynamic-feedback controller, the dimension of equation could be much higher than that of (10). In this case, we can compute the equilibrium solutions in an easier way. For instance, let us assume that we have a multiloop feedback system with an outer load-current loop and an inner-voltage loop. Depending on the type of converter and the performance requirements, we can also choose an inner inductor-current loop, which receives its reference from the voltage loop. Let the vectors \bar{X}^{C_l} , \bar{X}^{C_v} , and \bar{X}^{C_i} represent the states corresponding to the load-current loop, the inner-voltage loop, and the inner inductor-current loop, respectively. Rewriting

(13), we obtain

$$\begin{pmatrix} \dot{\bar{X}}^{C_l} \\ \dot{\bar{X}}^{C_v} \\ \dot{\bar{X}}^{C_i} \end{pmatrix} = \begin{pmatrix} A_{I_p} & A_{I_l} & 0 & 0 \\ A_{v_p} & A_{v_l} & A_{v_v} & 0 \\ A_{i_p} & A_{i_l} & A_{i_v} & A_{i_i} \end{pmatrix} \begin{pmatrix} \bar{X}^o \\ \bar{X}^{C_l} \\ \bar{X}^{C_v} \\ \bar{X}^{C_i} \end{pmatrix} + \begin{pmatrix} B^l \\ B^v \\ B^i \end{pmatrix} \bar{u} + \begin{pmatrix} B^{r_l} \\ B^{r_v} \\ B^{r_i} \end{pmatrix} v_r. \quad (52)$$

Setting the right-hand side of (52) equal to zero and solving the resulting equations, we obtain

$$\bar{X}^{C_i} = \Omega(\bar{X}^o). \quad (53)$$

Using (53), we rewrite the last equation of (21) as

$$d_j = \frac{1}{v_{ramp_j}} H_j^c \bar{X}^{C_i} = \Omega'(\bar{X}^o) \quad \text{or} \quad D = \Gamma(\bar{X}^o). \quad (54)$$

Substituting (54) into the first equation of (10) and setting $\bar{X}^o = 0$, we obtain

$$F(\bar{X}^o, \bar{u}) + G(\bar{X}^o, \bar{u})\Gamma(\bar{X}^o) + W_{1_{av}}^o(\bar{X}^o, \Gamma(\bar{X}^o)) = 0. \quad (55)$$

Unlike (51), (55) depends only on \bar{X}^o and hence is relatively easier to solve for the equilibrium solutions. Having obtained \bar{X}^o , we determine the equilibrium values of \bar{X}^{C_l} , \bar{X}^{C_v} , and \bar{X}^{C_i} using (53), thereby obtaining the equilibrium solutions of \bar{X} ($= \bar{X}_s$) for a given u ($= u_s$). Next we rewrite the last equation of (21) as

$$D = P(\bar{X}) \quad (56)$$

and rewrite the first equation of (21) as

$$\dot{\bar{X}} = F(\bar{X}, \bar{u}, v_r) + G(\bar{X}, \bar{u})P(\bar{X}) + W_{1_{av}}(\bar{X}, P(\bar{X})) = 0. \quad (57)$$

The stability of a given equilibrium solution \bar{X} is ascertained by the eigenvalues of the Jacobian matrix of the right-hand side of (57) evaluated at \bar{X}_s . To determine the postbifurcation scenario, we compute the normal form of (57) in the vicinity of the bifurcation point [21].

D. Analysis under Saturated Conditions

The unsaturated region for N parallel converters, operating with a finite but large frequency, is a boundary layer around the intersection of all of the N discontinuous hypersurfaces. The stability analysis (using bifurcation analyses and Lyapunov's method) performed so far assumes that the parallel converter is operating in this region. When one or more converters stop modulating for one or more switching cycles, then we have a saturated system.

If all of the converters are not modulating, the system is fully saturated; otherwise, the system is partially saturated. In a parallel converter with N switches, there are 2^N ways by which a full saturation can occur. For the same system, there are $\sum_{i=1}^{N-1} (N!/(N-1)!(i!))$ possibilities for partial saturation. Under full saturation, these piecewise-linear systems behave as autonomous systems because they are not switching. However, under partial saturation, the parallel converter still behaves as a nonlinear nonautonomous system because there is at least one converter, which is operating in the unsaturated region.

To analyze the stability of a saturated system, we need to address two issues. First, when a parallel converter, which is operating in the unsaturated region, saturates, does the solution remain inside the boundary layer or leave? Second, if the solution leaves the boundary layer, does the trajectory return back to it? The first issue deals with the question of existence; that is, under what conditions do all the solution trajectories point toward the boundary layer. If all the solution trajectories point toward the boundary layer for all values of the closed-loop states, then we have global existence of the boundary layer. The second issue, which deals with the reaching condition for the solution trajectories, becomes important in the absence of global existence of the boundary layer.

We deal with the issue of existence using Lyapunov's direct II method. The stability analysis using a positive definite smooth Lyapunov function V for a nonsmooth system with a discontinuous surface demands that the following three conditions are satisfied [22, 23]:

- 1) in the saturated/continuity region $\dot{V}(\cdot) < 0$;
- 2) as the solution approaches the discontinuity surface $\dot{V}(\cdot) \rightarrow 0$;
- 3) on the discontinuity surface $\dot{V}(\cdot) = 0$.

If these three conditions are satisfied, then the solution exists on the surfaces of discontinuity. The converters that we deal with have finite but large frequencies and hence have boundary layers around the discontinuity surfaces. If the width of the boundary layer is zero (when the switching frequency is infinite), the above conditions apply directly. These conditions do not, however, carry over to a finite-frequency converter, and at best give an upper estimate of stability. The reason is that, within the boundary layer, the nominal solution for the parallel converter is a periodic trajectory and not an equilibrium point, for which Lyapunov's method does not apply. For the stability analysis in this region, one needs to reduce the order of the system and then use Lyapunov's method or bifurcation analyses. We have shown this in the preceding sections.

Outside the boundary layer, however, the converters are not switching. Hence, the conditions

TABLE I
Nominal Parameters for the Two Buck Converter Modules

Parameters	Nominal Value
$L_1 = L_2$	50 μH
$r_{L_1} = r_{L_2}$	21 m Ω
$C_1 = C_2$	4400 μF
$r_{L_1} = r_{L_2}$	50 m Ω
$v_{r_1} = v_{r_2}$	2.0 V
$f_{i_1} = f_{i_2}$	1.0
$f_{v_1} = f_{v_2}$	0.4
$T = 1/\text{switching frequency}$	10 μsec ($= 1/100$ kHz)
$v_{\text{ramp}_1} = v_{\text{ramp}_2}$	3.0 V
u	20 V–50 V

for $\dot{V}(\cdot) < 0$ for a converter operating with no boundary layer are directly applicable to a finite-frequency, fully saturated converter, as long as the solutions are in the saturated region. For partial saturation, at least one of the converters is switching. To determine the stability of the quasi-solution surface, we resort to the discretized version of the three (Lyapunov-based) above conditions [20]. However, to accomplish this, we need to modify the nonlinear map for the unsaturated region.

To determine the reaching conditions for those trajectories that leave the boundary layer (if global existence cannot be established), we find the equilibrium solutions for the saturated converter. Using the first equation of (17), we show that the dynamics of a fully saturated system are given by

$$X_{k+1} = e^{A_{1\text{sat}}t_{1\text{sat}}} + (e^{A_{1\text{sat}}t_{1\text{sat}}} - I)A_{1\text{sat}}^{-1}B_{1\text{sat}}u_k + (e^{A_{1\text{sat}}t_{1\text{sat}}} - I)A_{1\text{sat}}^{-1}B_{1\text{sat}}^r v_r. \quad (58)$$

The equilibrium solutions of (58) are determined using the constraint $X_{k+1} = X_k = X_{\text{sat}}$. The result is

$$X_{\text{sat}} = (e^{A_{1\text{sat}}t_{1\text{sat}}} - I)^{-1}((e^{A_{1\text{sat}}t_{1\text{sat}}} - I)A_{1\text{sat}}^{-1}B_{1\text{sat}}u_k + (e^{A_{1\text{sat}}t_{1\text{sat}}} - I)A_{1\text{sat}}^{-1}B_{1\text{sat}}^r v_r). \quad (59)$$

If an equilibrium solution is virtual, then the error trajectories will be inside the boundary layer eventually. If it is real, then it will influence the unsaturated solution. For partially saturated systems, we can, similarly, determine the equilibrium solutions for the discretized system.

V. RESULTS

In the previous sections, we developed the methodologies and criteria for the stability analysis of parallel dc-dc pulsewidth modulated (PWM) converters (see Table I for parameter details) using different models. We applied these criteria to analyze the stability of two parallel buck converters (shown

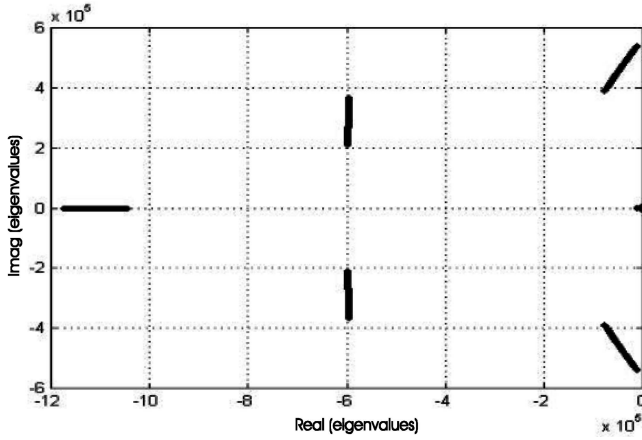


Fig. 3. Eigenvalues of averaged model for parallel converter indicate a stable system.

in Fig. 2) operating with ACS control. The states of the plant are i_{L1} , i_{L2} , v_{C1} , and v_{C2} . There are additional states corresponding to the load-current and voltage-loop controllers. Each of these converters has a multiloop control with an outer load-sharing current loop and an inner voltage loop. The objective of the closed-loop system is to share the load power equally and regulate the output voltage. It is worth noting that we can apply any other parallel-control scheme like the master-slave control, as well.

A. Unsaturated Control

We choose the control structure based on [14]. The compensators for the outer-loop current controllers have the form

$$\frac{\omega_{I_k}}{s} \left(\frac{\frac{s}{\omega_{I_{zk}}} + 1}{\frac{s}{\omega_{I_{pk}}} + 1} \right)$$

(nominal values: $\omega_{I_1} = \omega_{I_2} = 4 * 10^4$, $\omega_{I_{z1}} = \omega_{I_{z2}} = 2 * 10^3$, and $\omega_{I_{p1}} = \omega_{I_{p2}} = 1 * 10^4$), whereas the compensator structure for the inner-loop current controller has the form

$$\frac{\omega_{i_k}}{s} \left(\frac{\frac{s}{\omega_{i_{zk1}}} + 1}{\frac{s}{\omega_{i_{pk1}}} + 1} \right) \left(\frac{\frac{s}{\omega_{i_{zk2}}} + 1}{\frac{s}{\omega_{i_{pk2}}} + 1} \right)$$

(nominal values: $\omega_{i_1} = \omega_{i_2} = 1 * 10^6$, $\omega_{i_{z11}} = \omega_{i_{z21}} = 1 * 10^4$, $\omega_{i_{z12}} = \omega_{i_{z22}} = 5 * 10^4$, $\omega_{i_{p11}} = \omega_{i_{p21}} = 4 * 10^5$, and $\omega_{i_{p12}} = \omega_{i_{p22}} = 5 * 10^5$). In Fig. 3, we plot the eigenvalues of the linearized averaged model as the input voltage is varied from 25 to 50 V. Since none of the eigenvalues in Fig. 3 has a positive real part, we conclude that the nominal solution is locally stable for the input voltage range.

Next, we analyze the stability of the same system using a nonlinear map. We consider two cases: one for

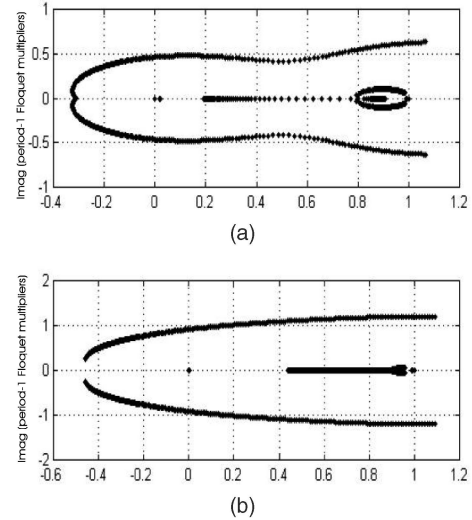


Fig. 4. Onset of instability in interleaved parallel buck converters. Two Floquet multipliers of period-one orbit exit unit circle away from real axis, indicating Hopf bifurcation. (a) With ESR. (b) Without ESR.

which the effect of the ESR of the output capacitors is considered and the other for which it is not. In Figs. 4(a) ($ESR \neq 0$) and 4(b) ($ESR = 0$), we show the Floquet multipliers of the linearized map for these two cases. For both cases, we see that, as the bifurcation parameter (input voltage) is increased, two complex conjugate Floquet multipliers exit the unit circle away from the real axis, indicating a Hopf bifurcation. This slow-scale instability is not observed in Fig. 3. To find out the type of bifurcation, we compute the normal form of the nonlinear map in the neighborhood of the bifurcation point. The normal form indicates a subcritical Hopf bifurcation. Using a second-order Poincare map we show that the postbifurcation response is quasiperiodic. This is evident in Fig. 5.

Fig. 6 shows the impact of variations in the output capacitance on the instability mechanism of the interleaved parallel-buck converters. Starting with the nominal values for C_1 and C_2 , we reduce their magnitudes by a factor of two for each successive set of data, keeping all of the other parameters constant. For each set of capacitor values, we investigate the stability of the system for an input voltage varying from 25 to 50 V. For values of the output capacitance close to the nominal value, a subcritical Hopf bifurcation occurs as the input voltage is increased. As the value of the output capacitor is reduced, no local instability occurs for the input-voltage variation. However, as the output capacitance is reduced even further, the parallel converter loses stability as the input voltage is increased. We found that the instability occurs due to a supercritical Hopf bifurcation and not due to a subcritical Hopf bifurcation.

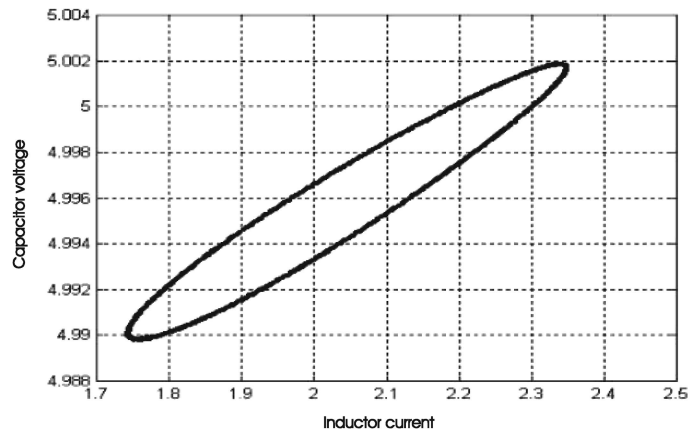


Fig. 5. Post-Hopf bifurcation scenario of interleaved parallel buck converters. Second-order Poincare map clearly shows quasiperiodic response. It shows that even after the onset of instability, voltage ripple magnitude is not drastically large; as such, converter can be operated close to the boundary, thereby increasing its dynamic response and bandwidth.

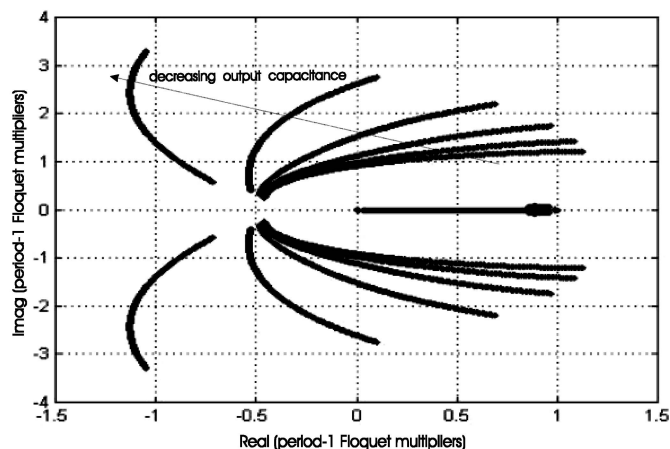


Fig. 6. Impact of variations in output capacitance on mechanism of instability of interleaved parallel converters. As capacitance is decreased, mechanism for instability of parallel converter changes from supercritical to subcritical Hopf bifurcation (ascertained using the normal in (43)). Subcritical Hopf bifurcation leads to slow-scale instability.

Next, we consider the impact of variations in the input voltage on the operation of two parallel-buck converters operating in phase rather than with a phase shift of 180° . We find that, for the same nominal parameters (as considered above), the synchronized converters are stable for the entire input voltage range. However, for a higher gain of the voltage-loop controller, we observe the onset of a fast-scale instability with a increasing input voltage. The fast-scale instability occurs in the form of a period-doubling bifurcation, as shown in the bifurcation diagram in Fig. 7, which ultimately leads to chaos as the input voltage is increased beyond 50 V. In Fig. 8, we show the movement of the Floquet multipliers of the period-one orbit. As the input voltage is increased, one of the Floquet multipliers exits the unit circle through -1 , indicating a period-doubling bifurcation. A second-order nonlinear map [9] reveals that the period-doubling bifurcation is supercritical in nature.

B. Saturated Control

Finally, we demonstrate the behavior of two parallel-buck converters operating with a multiloop static feedback controller under saturated conditions. We discuss in detail only the cases when both switches are turned off. We can extend the same technique for the other three cases of full saturation. In a subsequent paper, we will demonstrate how to extend these concepts to converters operating under partial saturation and operating with dynamic feedback controllers. Mazumder, et al. [24] present a sliding-mode control scheme for parallel-buck and parallel-boost converters that guarantees stability on all of the hyperplanes and their intersections.

To demonstrate our point, we consider only the Hamiltonian part of the system. The presence of the parasitic resistors makes the system more passive [25, 26]. In addition, we change the control strategy from load-current equalization to line-current

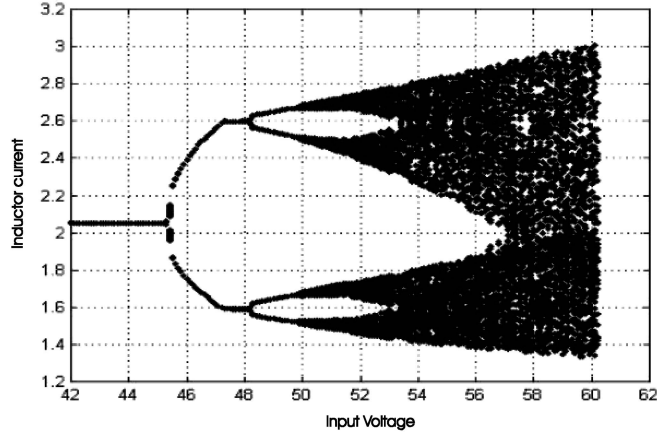


Fig. 7. Bifurcation diagram of closed-loop parallel buck converter operating in phase. It shows a fast-scale instability.

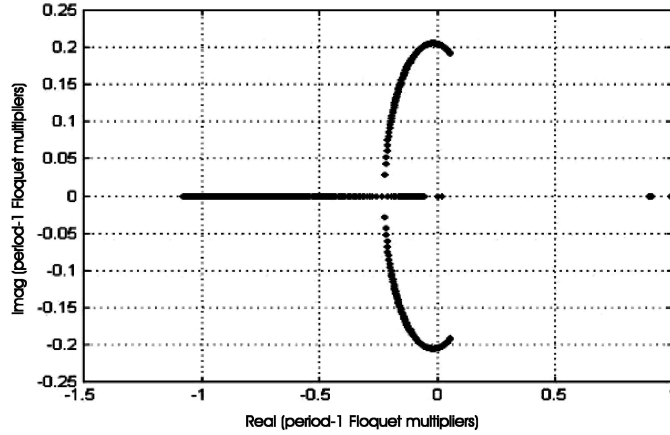


Fig. 8. One of the Floquet multipliers of period-one orbit exits the unit circle via -1 , indicating period-doubling bifurcation.

equalization. For the buck converter, this change does not alter the control objectives, which are to regulate the capacitor voltage and share the load power equally. However, with these two simple changes, we prove our point more easily.

For the closed-loop parallel converter operating with static-feedback controllers, the switches S_1 and S_2 are turned off if the error signals of the controller are less than zero. In this continuity region, the error signals are given by

$$\sigma_k = g_{v_k} \left(v_r - f_{v_1} v_{C_k} + g_{i_k} f_{i_k} \left(\frac{1}{2} \sum_{j=1}^2 i_{L_j} - i_{L_k} \right) \right), \quad k = 1, 2. \quad (60)$$

In (60), f_{v_k} are the feedback-sensor gains for the output voltages, f_{i_k} are the feedback-sensor gains for the inductor currents, g_{v_k} and g_{i_k} are the voltage- and current-loop gains of the two buck-converter modules. We choose the following Lyapunov function in the continuity region:

$$V(\sigma_1, \sigma_2) = \frac{1}{2} \sigma^T D \sigma = \frac{1}{2} (\sigma_1 \ \sigma_2) \begin{pmatrix} 1 & 0 \\ 0 & 1 \end{pmatrix} (\sigma_1 \ \sigma_2)^T. \quad (61)$$

Therefore,

$$\begin{aligned} \dot{V}(\sigma_1, \sigma_2) &= g_{v_1} \left(v_r - f_{v_1} v_{C_1} + g_{i_1} f_{i_1} \left(\frac{1}{2} \sum_{j=1}^2 i_{L_j} - i_{L_1} \right) \right) \\ &\quad \times \left(\frac{g_{v_1} g_{i_1} f_{i_1}}{2} (i_{L_2} - i_{L_1}) - g_{v_1} f_{v_1} \dot{v}_{C_1} \right) \\ &\quad + g_{v_2} \left(v_r - f_{v_2} v_{C_2} + g_{i_2} f_{i_2} \left(\frac{1}{2} \sum_{j=1}^2 i_{L_j} - i_{L_2} \right) \right) \\ &\quad \times \left(\frac{g_{v_2} g_{i_2} f_{i_2}}{2} (i_{L_1} - i_{L_2}) - g_{v_2} f_{v_2} \dot{v}_{C_2} \right). \quad (62) \end{aligned}$$

Using the constraint $v_{C_1} = v_{C_2} = v_C$, the equations for the Hamiltonian system

$$\dot{i}_{L_k} = -\frac{v_C}{L_k} + \frac{S_k u}{L_k}, \quad \forall \quad k = 1, 2 \quad (63a)$$

$$\dot{v}_C = \sum_{j=1}^2 \frac{i_{L_j}}{C_1 + C_2} - \frac{v_C}{(C_1 + C_2)R} \quad (63b)$$

and assuming $S_1 = S_2 = 0$ and gains of the two modules are the same for simplicity (i.e., $g_{i_1} = g_{i_2} = g_i$, $g_{v_1} = g_{v_2} = g_v$, $f_{i_1} = f_{i_2} = f_i$, and $f_{v_1} = f_{v_2} = f_v$), we

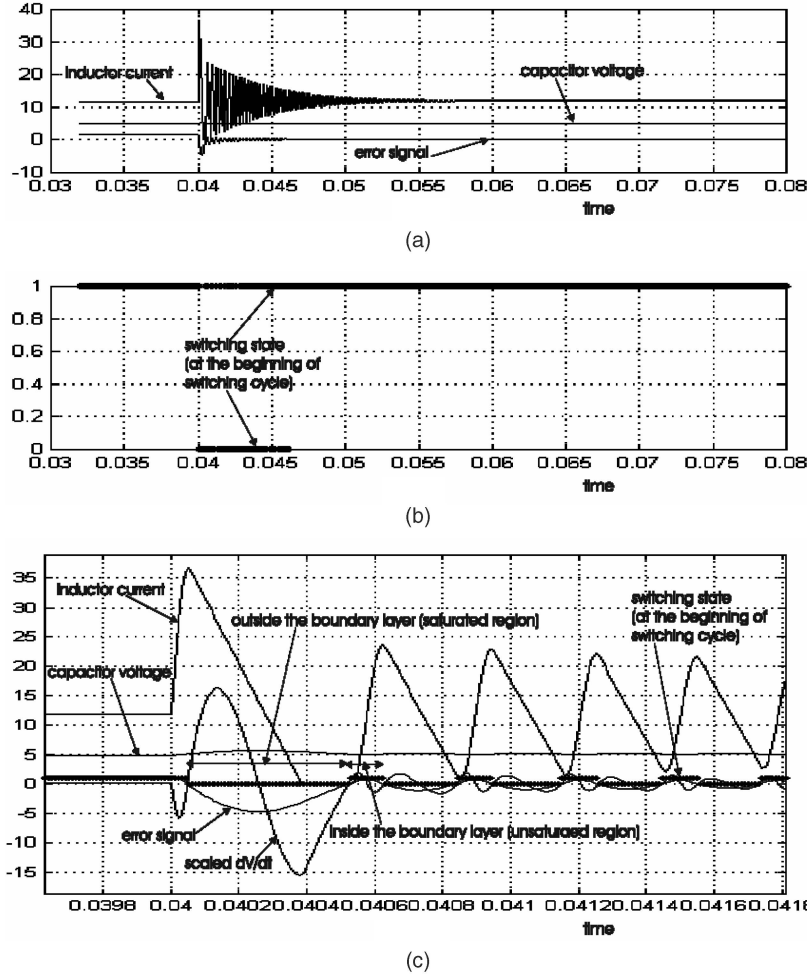


Fig. 9. Stability analysis, based on unsaturated model, predicts a stable equilibrium before and after feedforward disturbance. However, during transients, system saturates. As a result, existence condition $\dot{V}(\sigma_1, \sigma_2) < 0$ is violated. Although error trajectories return back to sliding manifold (as predicted and as illustrated in (b) by switching states that are sampled once in every switching cycle), transient performance is unacceptable. Part (c) is expansion of transient region in (a) and (b). We note that, in a practical converter, the fault-protection mechanism will shut down the converter because of large current swings. In other words, the above result demonstrates that stability alone does not guarantee performance [24].

obtain

$$\begin{aligned} \dot{V}(\sigma_1, \sigma_2)(S_1 = S_2 = 0) &= \frac{2g_v^2 f_v}{C_1 + C_2} (v_r - f_v v_C) \left(\frac{v_C}{R} - i_{L_1} - i_{L_2} \right) \\ &+ \frac{g_v^2 g_i^2 f_i}{2} \left(\frac{1}{L_1} - \frac{1}{L_2} \right) (i_{L_2} - i_{L_1}) v_C. \end{aligned} \quad (64)$$

When the two modules have the same parameters, the second term in (64) vanishes. Using (64), we can show that when the two converters have the same parameters, the error trajectories in the continuity region, given by $S_1 = S_2 = 0$, will move toward the boundary layer provided that $(v_C/R) > i_{L_1} + i_{L_2}$. Now, the closed-loop parallel converter (with the same parameters) operates in the saturated region given by $S_1 = S_2 = 0$ only if $v_r > f_v v_C$. However, the equilibrium solutions of (63) when $S_1 = S_2 = 0$ are $i_{L_1} = i_{L_2} = 0$ and $v_C = 0$. Therefore, the equilibrium solution is virtual. In other words, the closed-loop converter

cannot remain in this saturated region permanently.

Next, we consider two cases to demonstrate these two points. First, we consider a parallel-buck converter with $C_1 = C_2 = 4400 \mu\text{F}$ and $L_1 = L_2 = 50 \mu\text{H}$. For the second case, we change only the value of the output capacitor to $100 \mu\text{F}$. We find that the (unsaturated) nominal solution of the converter in case one is stable for an input voltage range of 70 V, starting at 20 V. The converter in the second case has a stable (unsaturated) nominal solution at 20 V. However, the nominal solution is unstable at 90 V. Let us assume that initially these converters are operating in steady state with an input voltage of 20 V. We then subject them to a feedforward disturbance so that the final input voltage is 90 V. The disturbance is deliberately chosen to be strong enough so that the two switches turn off. In other words, $S_1 = 0$ and $S_2 = 0$.

Fig. 9 shows the results for case one. We see that the converter is stable before and after the feedforward

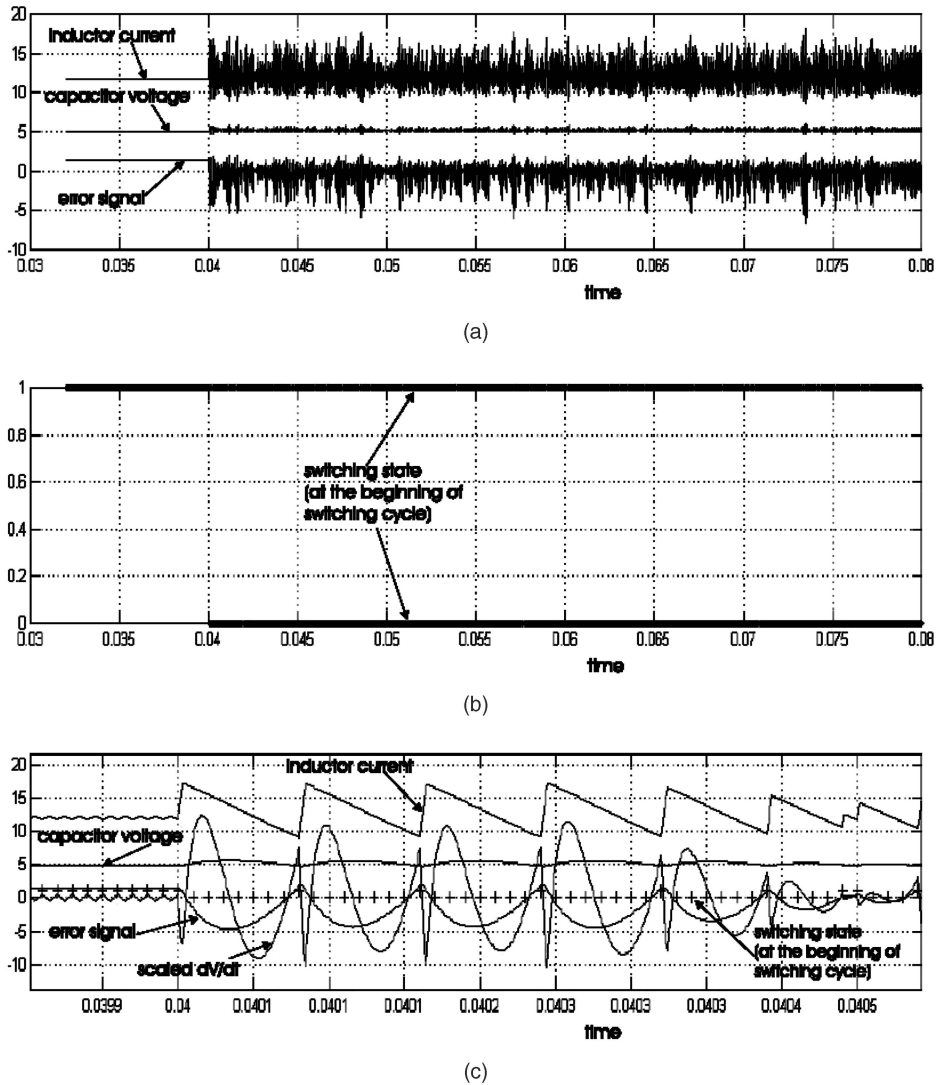


Fig. 10. Stability analysis which predicts that, while the parallel converter is stable before the disturbance, the postdisturbance dynamics are unstable. Inside, there is chaotic attractor inside the boundary layer (which is clearly illustrated in (b) by switching states that never stabilize). Part (c) is an expansion of (a) and (b) in the region immediately after the disturbance.

disturbance. We predicted this based on the reaching condition and the stability of the (unsaturated) equilibrium solution. After the disturbance, when the system saturates, $\dot{V}(\sigma_1, \sigma_2)$ becomes positive because $(v_C/R) > i_{L_1} + i_{L_2}$. As a result, the error trajectories move away from the boundary layer. Since the equilibrium solution in the saturated region is virtual, the error trajectories approach the boundary layer when $\dot{V}(\sigma_1, \sigma_2)$ is less than zero, and eventually modulation begins. The states of the system indicate a damped oscillatory behavior before settling down because the nominal solution is a stable focus.³

Fig. 10 shows the results for case two. It shows that, while the parallel converter is stable before the disturbance, the postdisturbance dynamics are

³We note that in a practical converter, the system will shutdown due to fault protection well before the currents attain the large values in Fig. 9.

unstable. We know that the error trajectories cannot stay in the saturated region given by $S_1 = 0$ and $S_2 = 0$. However, inside the boundary layer, instead of a stable nominal solution, we have a chaotic attractor. Hence the dynamics of the converter after the disturbance are chaotic. The switching function in Fig. 10(b) confirms this. We also see from Fig. 10(c) that the derivative of the Lyapunov function correctly predicts the dynamics of the error trajectories.

We make two observations based on the results of cases one and two. First, for the same feedforward disturbance, the derivative of the Lyapunov function for case two spends much less time in the saturated region as compared with case one. This is because, for the second case, the voltage across the capacitor (for a given load), due to its smaller size, changes more rapidly with changes in the inductor current. We can verify this by neglecting the second term in (64). Second, although a reduction in the capacitance gives

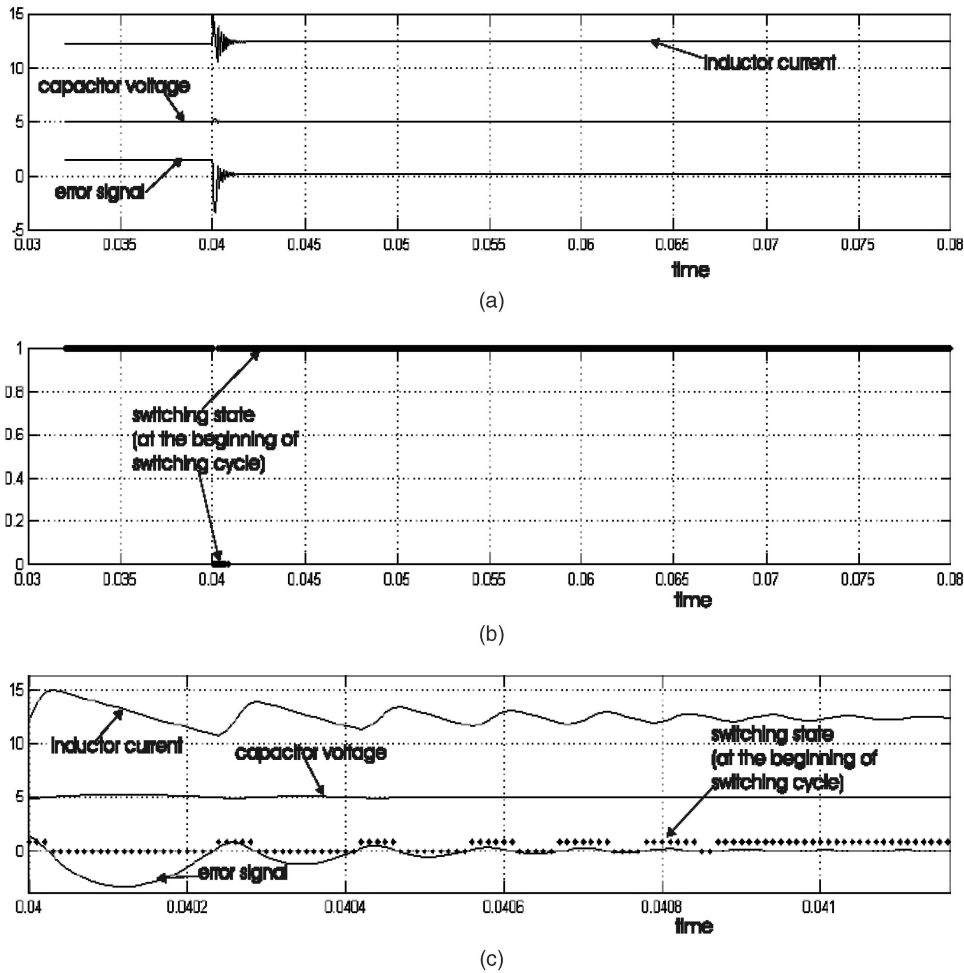


Fig. 11. Properly designed parallel converter. It has excellent steady-state and transient performances.

a better dynamic response, it results in an unstable nominal solution. In Fig. 11, we show the steady-state and dynamic performances of the parallel converter with $L_1 = L_2 = 250 \mu\text{H}$ and $C_1 = C_2 = 400 \mu\text{F}$. This simple compromise, guided by $\dot{V}(\sigma_1, \sigma_2)$ and the stability analysis of the nominal solution, gives a better dynamic response.

So far we have considered identical converters. We now consider a case in which the two converters have about a 5% difference in the line inductance. Converter one has a line inductance of $250 \mu\text{H}$, whereas converter two has a line inductance of $235 \mu\text{H}$. The output capacitances of both converters are chosen to be $400 \mu\text{F}$. We keep the values of the rest of the parameters, except g_i , the same as those in the other three cases. Because the inductors of the two converters are not identical, the term representing the differences in the two inductor currents in (64) is important. Equation (64) shows that, unless these terms are bounded and small, the dynamics of these two parallel converters, even with a small variation in the parameter of one power stage, can be vastly different from the ideal system. In this case, one simple way to achieve load sharing would be to keep

g_i small. However, too small a value of g_i would nullify load sharing.

In Fig. 12, we show the steady-state and dynamic performances of the parallel converter with a suitable choice of g_i . The nominal solution of the system for the entire input voltage range is stable. Although the values of the inductors of the two modules are different, the performance of the system is similar to that of the ideal case. There is, however, a minor difference in the switching sequences. In the case of the ideal converters, both switching states are identical. Hence, the system switches between the unsaturated and saturated regions given by $S_1 = S_2 = 0$. However, now, due to the parametric difference of the converters, both of the error trajectories do not enter or exit the boundary layer at the same time. Hence, there is a time span during which the system is partially saturated before it operates in the unsaturated region. During this time, S_1 is turned off while S_2 modulates. We obtained the switching sequence $S_1 = 0, S_2 = 0 \rightarrow S_1 = 0, S_2 \in (0, 1) \rightarrow S_1 \in (0, 1), S_2 \in (0, 1)$ only because $\gamma (= i_{L_1} - i_{L_2})$ is constrained by a proper choice of g_i . For progressively larger values of g_i , we would obtain the switching sequences $S_1 = 0, S_2 =$

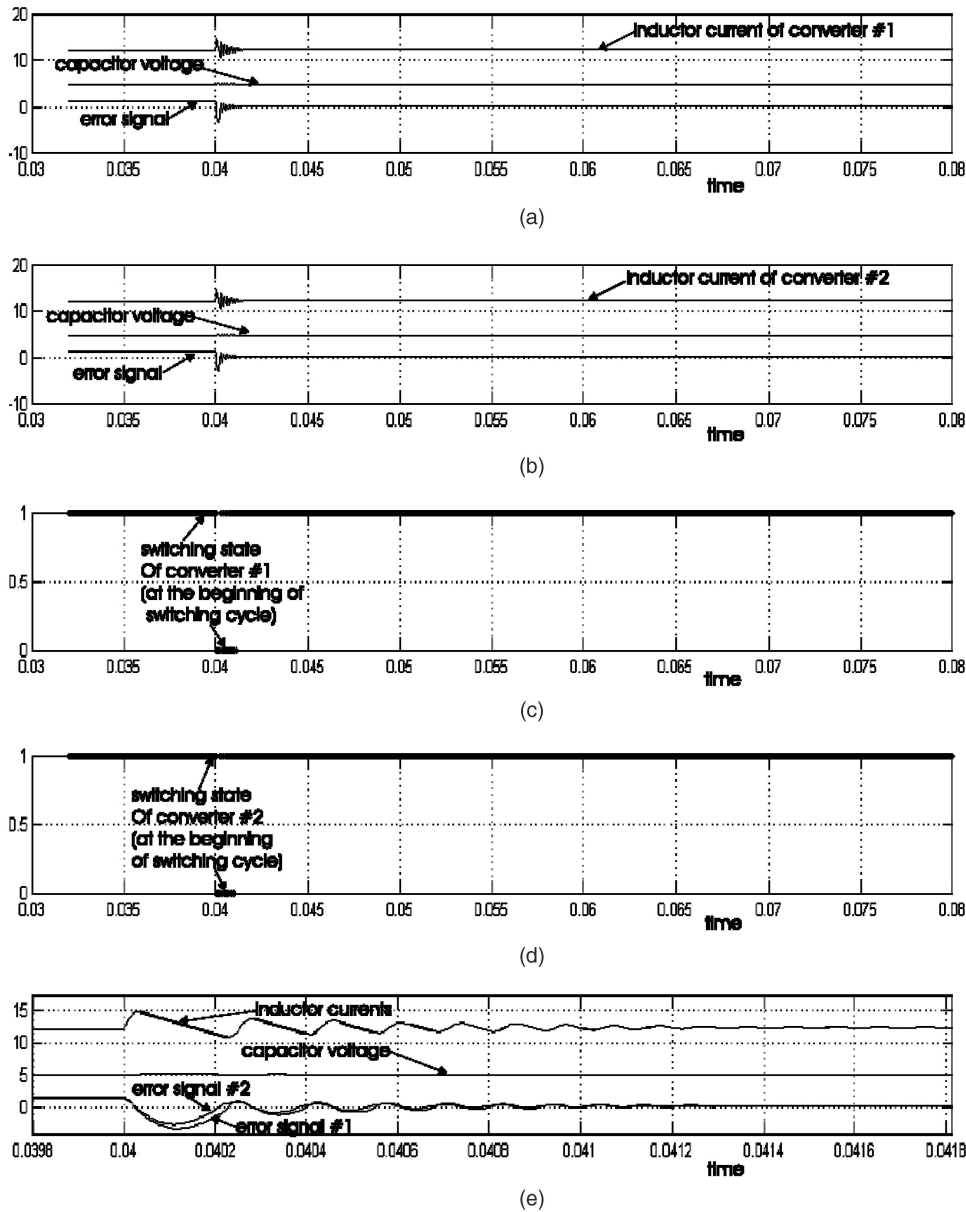


Fig. 12. Performance of parallel converter under parametric variation. Although the two error trajectories enter the unsaturated region at different times, a careful design consideration (based on Lyapunov function) results in a system with high performance. Part (c) is an expansion of the transient region in (a) and (b).

$1 \rightarrow S_1 \in (0, 1), S_2 = 1$ or $S_1 = 0, S_2 = 1, S_1 = 1, S_2 = 1$ after the disturbance. This results in a deterioration of the steady-state and dynamic performance of the system.

VI. SUMMARY AND CONCLUSION

We investigate the local and global stability of parallel dc-dc converters in the unsaturated and saturated regions. Using a nonlinear map, we demonstrate the fast-scale and slow-scale instabilities in two parallel converters. The averaged model cannot predict the fast-scale dynamics. Using a bifurcation analysis (with the input voltage as the bifurcation parameter) based on a nonlinear map,

we show how the type of instability changes when the converters operate using interleaving instead of operating in phase. The state-space averaged model cannot distinguish between the converters operating in phase from those operating using interleaving. For the interleaved converter, we show how the mechanism of instability changes from a subcritical Hopf bifurcation to a supercritical bifurcation as the values of the output capacitors are decreased. Using a second-order Poincare map, we find that the post-Hopf bifurcation dynamics are quasiperiodic.

To determine the postbifurcation dynamics in the vicinity of the nominal solution, one can use either a higher order map, numerical techniques, or the normal form of the system of equations. We used the first two

methods for standalone converters [9]. Because the dimensionality of the closed-loop parallel converter is, in general, higher than that of standalone converters, the normal form may be a better alternative. In this paper, we have outlined a technique to generate the normal form of a closed-loop system described by a nonlinear map. We will discuss this methodology, in detail, in another paper.

We also outline ways to determine the stability of saturated regions, which we demonstrate using two synchronized parallel buck converters. Using a positive definite Lyapunov function, we show that, for a fully saturated parallel converter, the dynamics of the system in the saturated region are governed by the derivative of the Lyapunov function. When the derivative of the Lyapunov function is negative, the error trajectories approach the boundary layer. When the derivative is positive, the error trajectories leave the saturated region. In this case, we show that if the equilibrium solutions of the saturated regions are virtual, these trajectories will ultimately reach the boundary layer.

Finally, we apply these concepts of stability for the saturated and unsaturated regions to four cases. For the first three cases, we consider the parameters of the parallel converters to be the same. We show, using cases one and two, that the nominal solution (in the unsaturated region) is stable if and only if the dynamics of the system in the saturated and unsaturated regions are stable. That is why, while the postdisturbance steady-state dynamics of the closed-loop system in case one are stable, they are chaotic for the second case. However, we find that the transient dynamics for case one are much more oscillatory than those of case two. We explain this using the derivative of the Lyapunov function. Based on these two cases, we show in case three how easily one can improve the transient and steady-state performances of the system. For the fourth case, we consider two parallel buck converters with parametric variation. Using (64), we show how to tune the outer-loop current gain g_i so that the performance of the nonideal system is close to the ideal case. We also show how and why the switching sequence changes with increasing g_i .

APPENDIX A. AVERAGE MODEL FOR TWO PARALLEL BUCK CONVERTERS

In each switching cycle (of duration T), there are four subintervals (see Fig. 13). The switching sequence in each switching cycle is $S_1 = 1, S_2 = 0 \rightarrow S_1 = 0, S_2 = 0 \rightarrow S_1 = 0, S_2 = 1 \rightarrow S_1 = 0, S_2 = 0$. Using (4), we obtain the following state-space

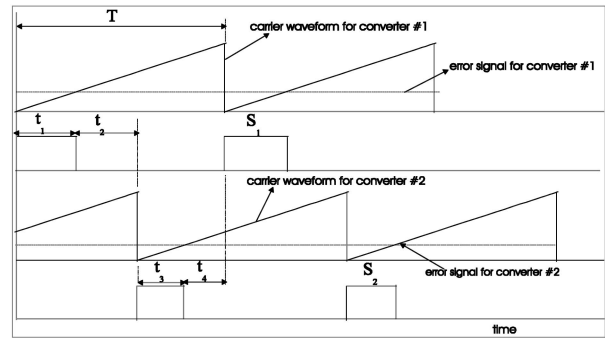


Fig. 13. Interleaved converters.

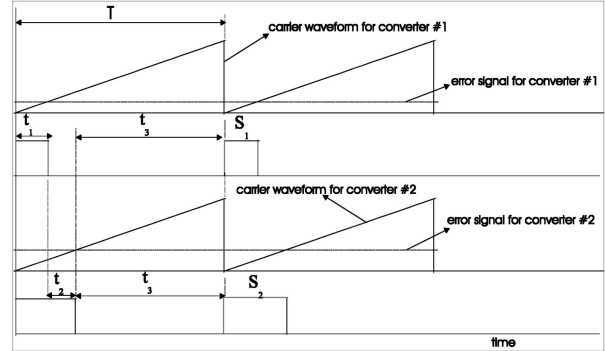


Fig. 14. Synchronized (in-phase) converters.

equations for these four subintervals:

$$\begin{aligned} \dot{X}^o &= A_{10}^o X^o + B_{10}^o u, & t < t_1 \\ \dot{X}^o &= A_{00}^o X^o + B_{00}^o u, & t_1 < t < t_1 + t_2 \\ \dot{X}^o &= A_{01}^o X^o + B_{01}^o u, & t_1 + t_2 < t < t_1 + t_2 + t_3 \\ \dot{X}^o &= A_{00}^o X^o + B_{00}^o u, & t_1 + t_2 + t_3 < t < T. \end{aligned} \quad (65)$$

For the dc-dc buck converter, $A_{10}^o = A_{00}^o = A_{01}^o = A^o$ and $B_{00}^o = 0$. Averaging the four equations in (65) yields

$$\dot{X}^o = A^o X^o + \left(\frac{t_1}{T} B_{10}^o + \frac{t_3}{T} B_{01}^o \right) u. \quad (66)$$

The duty ratio for the two buck converters of the parallel module are defined by $d_1 = t_1/T$ and $d_2 = t_3/T$, respectively. Rewriting (66) in terms of d_1 and d_2 , one obtains the following averaged model:

$$\dot{X}^o = A^o X^o + (d_1 B_{10}^o + d_2 B_{01}^o) u. \quad (67)$$

In each switching cycle (of duration T), there are four subintervals (see Fig. 14). The switching sequence in each switching cycle is $S_1 = 1, S_2 = 1 \rightarrow S_1 = 0, S_2 = 1 \rightarrow S_1 = 0, S_2 = 0$. Using (4), we obtain the following state-space equations for these three subintervals:

$$\begin{aligned} \dot{X}^o &= A_{11}^o X^o + B_{11}^o u, & t < t_1 \\ \dot{X}^o &= A_{01}^o X^o + B_{01}^o u, & t_1 < t < t_1 + t_2 \\ \dot{X}^o &= A_{00}^o X^o + B_{00}^o u, & t_1 + t_2 < t < T. \end{aligned} \quad (68)$$

For the dc-dc buck converter, $A_{11}^o = A_{01}^o = A_{00}^o = A^o$ and $B_{00}^o = 0$. Averaging the three equations in (68) yields

$$\dot{X}^o = A^o X^o + \left(\frac{t_1}{T} B_{11}^o + \frac{t_1 + t_2}{T} B_{01}^o \right) u. \quad (69)$$

The duty ratio for the two buck converters of the parallel module are defined by $d_1 = t_1/T$ and $d_2 = (t_1 + t_2)/T$, respectively. Rewriting (69) in terms of d_1 and d_2 , one obtains the following averaged model:

$$\dot{X}^o = A^o X^o + (d_1 B_{11}^o + d_2 B_{01}^o) u. \quad (70)$$

REFERENCES

- [1] Nayfeh, A. H., and Balachandran, B. *Applied Nonlinear Dynamics*. New York: Wiley, 1995.
- [2] Khalil, H. K. *Nonlinear Systems*. Englewood Cliffs, NJ: Prentice-Hall, 1996.
- [3] Aubin, J., and Cellina, A. *Differential Inclusions: Set-Valued Maps and Viability Theory*. New York: Springer-Verlag, 1984.
- [4] Filippov, A. F. *Differential Equations with Discontinuous Righthand Sides*. Boston, Kluwer, 1988.
- [5] Utkin, V. *Sliding Modes in Control Optimization*. New York: Springer-Verlag, 1992.
- [6] Deane, J. H. B., and Hamill, D. C. Analysis, simulation and experimental study of chaos in the buck converter. In *Proceedings of IEEE Power Electronics Specialists Conference*, 1990, 491–498.
- [7] Tse, C. K. Flip bifurcation and chaos in three-state boost switching regulators. *IEEE Transactions on Circuits and Systems-1: Fundamental Theory and Applications*, **41** (1994), 16–23.
- [8] Banerjee, S., Ott, E., Yorke, J. A., and Yuan, G. H. Anomalous bifurcations in dc-dc converters: Borderline collisions in piecewise smooth maps. In *Proceedings of IEEE Power Electronic Specialists Conference*, 1997, 1337–1344.
- [9] Mazumder, S. K., Nayfeh, A. H., and Boroyevich, D. A theoretical and experimental investigation of the fast- and slow-scale instabilities of a dc-dc converter. *IEEE Transactions on Power Electronics*, **16**, 2 (2001), 201–216.
- [10] Middlebrook, R. D., and Cuk, S. A general unified approach to modeling switching-converter power stages. In *Proceedings of IEEE Power Electronic Specialists Conference*, 1977, 521–550.
- [11] Lee, F. C. Modeling, Analysis, and Design of PWM Converter. Virginia Power Electronic Center Publications Series, vol. 2, Blacksburg, VA, 1990.
- [12] Rajagopalan, J., Xing, K., Guo, and Lee, F. C. Modeling and dynamic analysis of paralleled dc/dc converters with master/slave current sharing control. In *Proceedings of IEEE Applied Power Electronics Conference*, 1996, 678–684.
- [13] Kohama, T., Ninomiya, T., Shoyama, M., Ihara, F. Dynamic analysis of parallel-module converter system with current balance controllers. In *Proceedings of International Telecommunications Energy Conference*, 1994, 190–195.
- [14] Thottuvelli, V. J., and Verghese, G. C. Stability analysis of paralleled dc/dc converters with active current sharing. In *Proceedings of IEEE Power Electronics Specialists Conference*, 1996, 1080–1086.
- [15] Parker, T. S., and Chua, L. O. *Practical Numerical Algorithms for Chaotic Systems*. New York: Springer-Verlag, 1989.
- [16] Royden, H. L. *Real Analysis*. Englewood Cliffs, NJ: Prentice-Hall, 1988.
- [17] Dennis, J. E., Jr., and Schnabel, R. B. *Numerical Methods for Unconstrained Optimization and Nonlinear Equations*. Englewood Cliffs, NJ: Prentice-Hall, 1983.
- [18] Salon, S. J. Computer Methods in Electrical Power Engineering. Dept. of Electrical Power Engineering, Rensselaer Polytechnic Institute, Troy, NY, Class notes, 1993.
- [19] Watson, L. T. Globally convergent homotopy algorithms for nonlinear systems of equations. *Nonlinear Dynamics*, **1** (1990), 143–191.
- [20] Brogliato, B. *Nonsmooth Impact Mechanics: Models, Dynamics and Control*. New York: Springer-Verlag, 1996.
- [21] Nayfeh, A. H. *Method of Normal Forms*. New York: Wiley Interscience, 1993.
- [22] Shevitz, D., and Paden, B. Lyapunov stability theory of nonsmooth systems. *IEEE Transactions on Automatic Control*, **39** (1994), 1910–1914.
- [23] Wu, Q., Onyshko, S., Sepehri, N., and Thornton-Trump, A. B. On construction of smooth Lyapunov functions for non-smooth systems. *International Journal of Control*, **69** (1998), 443–457.
- [24] Mazumder, S. K., Nayfeh, A. H., and Boroyevich, D. Robust control of parallel dc-dc buck converters by combining integral-variable structure and multiple-sliding-surface control schemes. *IEEE Transactions on Power Electronics*, **17**, 3 (2002), 428–437.
- [25] Sanders, S. Nonlinear control of switching power converters. Ph.D. dissertation, Dept. of Electrical and Computer Engineering, Massachusetts Institute of Technology, Cambridge, MA, 1989.
- [26] van der Schaft, A. J. *L₂-Gain and Passivity Techniques in Nonlinear Control*. New York: Springer, 1996.
- [27] Siri, K. Analysis and design of distributed power systems. Ph.D. dissertation, Dept. of Electrical Engineering, University of Illinois at Chicago, IL, 1991.
- [28] Siri, K., Lee, C. Q., and Wu, T. F. Current distribution control for parallel-connected converters. *IEEE Transactions on Aerospace and Electronic Systems*, **28**, 3 (1992), 829–850.

- [29] Panov, Y., and Jovanovic, M. M.
Stability and dynamic performance of current-sharing control of paralleled voltage regulator modules. *IEEE Transactions on Power Electronics*, **17**, 2 (2002), 172–179.
- [30] Abu-Qahouq, J. A., Hong Mao, and Batarseh, I.
Novel control method for multiphase low-voltage high-current fast-transient VRMs. In *Proceedings of IEEE Power Electronics Specialists Conference, 2002*, 1576–1581.
- [31] Mazumder, S. K., and Nayfeh, A. H.
A new approach to the stability analysis of boost power-factor-correction circuits. *Journal of Vibrations and Control, Special Issue on Nonlinear Controls and Dynamics*, **9** (2003), 749–773.
- [32] Mazumder, S. K., Nayfeh, A. H., and Boroyevich, D.
A nonlinear approach to the analysis of stability and dynamics of standalone and parallel dc-dc converters. *Annual Proceedings of the Center for Power Electronics Systems*, (2000), 610–616. Also in Stability analysis of parallel dc-dc converters using a nonlinear approach. *IEEE Power Electronics Specialists Conference, 2001*, 1283–1288.
- [33] Iu, H. H. C., and Tse, C. K.
Bifurcation behavior in parallel-connected buck converters. *IEEE Transactions on Circuits and Systems I*, **48** (2002), 233–240.



Sudip K. Mazumder (M'01—SM'04) is the Director of Laboratory for Energy and Switching-Electronics Systems (LESES) and an assistant professor in the Department of Electrical and Computer Engineering at the University of Illinois, Chicago. He received his Ph.D. and M.S. degrees from Virginia Polytechnic Institute and State University, Blacksburg, Virginia and Rensselaer Polytechnic Institute, Troy, New York, in 2001 and 1993, respectively. He has over 10 years of professional experience and has held R&D and design positions in leading industrial organizations. His current areas of interests are interactive power-electronics/power networks, renewable and alternate energy systems, and new device and systems-on-chip enabled higher power density.

Dr. Mazumder received the ONR Young Investigator Award, NSF CAREER, and the DOE SECA awards in 2005, 2003, and 2002, respectively. He also received the Prize Paper Award from the *IEEE Transactions on Power Electronics* and the IEEE PELS in 2002. He is an associate editor for the *IEEE Transactions on Industrial Electronics* and *IEEE Power Electronics Letters*. He has published over 50 refereed and invited journal and conference papers and is a reviewer for 6 international journals.